Integrated ultrasonic particle positioning and low excitation light fluorescence imaging

A. L. Bernassau,[a] M. Al-Rawhani,[a] J. Beeley, and D. R. S. Cumming
School of Engineering, University of Glasgow, Glasgow, G12 8LT, United Kingdom

(Received 9 October 2013; accepted 25 November 2013; published online 10 December 2013)

A compact hybrid system has been developed to position and detect fluorescent micro-particles by combining a Single Photon Avalanche Diode (SPAD) imager with an acoustic manipulator. The detector comprises a SPAD array, light-emitting diode (LED), lenses, and optical filters. The acoustic device is formed of multiple transducers surrounding an octagonal cavity. By stimulating pairs of transducers simultaneously, an acoustic landscape is created causing fluorescent micro-particles to agglomerate into lines. The fluorescent pattern is excited by a low power LED and detected by the SPAD imager. Our technique combines particle manipulation and visualization in a compact, low power, portable setup. © *2013 AIP Publishing LLC*.
[http://dx.doi.org/10.1063/1.4846395]

The ability to control cells and micro-particles into specific patterns while simultaneously monitoring and extracting analytical indicators about the state and the physiology of the patterned cells is critical for a wide range of biological studies such as tissue engineering and cell culturing.[1,2] It has been shown that cells can be positioned onto the active area of ion-sensitive field-effect-transistor (ISFETs) integrated dielectrophoretic electrodes[3,4] for pH environment monitoring.[3,4] Quantitative immuno-fluorescent imaging is an alternative approach, as it provides an intracellular indicator of the metabolism and physiology of the cells in response to specific substances.[5] This approach requires a fluorescence microscope incorporating high power excitation source such as a mercury or xenon lamp.[6] An important part of such a microscope is the charge-coupled device (CCD) imager, often cooled, that is used to capture the fluorescence images of the patterned particles. To obtain clear images with this system, it is commonly achieved by increasing the intensity of excitation light or the concentration of the fluorophores. A significant drawback of this approach is that it increases the generation of reactive oxygen species (ROS) such as singlet oxygen that in turn will damage the cell (phototoxicity) and increase the rate of photo bleaching of the fluorophore itself.[6] Furthermore, the physical bulk of commercial fluorescence microscopes and substantial power required for excitation make this approach unsuitable for applications requiring compactness and/or low excitation power.

A significant improvement can be achieved using a Single Photon Avalanche Diodes (SPAD) array, an ultra-sensitive imager capable of detecting emitted fluorescence light at photon counting level, and thus permitting the use of low power excitation sources. In addition, SPADs, unlike CCD based imagers, do not require cooling, and are fabricated in Complementary Metal Oxide Semiconductor (CMOS) technology,[7,8] allowing miniaturisation and integration.

In this Letter, we demonstrate a compact, low power-excitation, fluorescence imager used in conjunction with an acoustic pattering device. The proposed integration enables pattering and positioning of micro-scale fluorescent particles while at the same time optically recording the patterns formed by the particles using low excitation source. The acoustic positioning element is based on acoustic standing waves and the fluorescence imager based on a 32×32 SPAD array detectors.

The block diagram of the complete system is shown in Fig. 1. The upper part of the setup is the acoustic device which employs multiple transducers surrounding an octagonal cavity and mounted by a 3-D micro-positioner; the lower part hosts the detector which consists of the SPAD imager, a fluorescence interference cube, an (18°) viewing angle light-emitting diode (LED) (Optek Technology, USA, OVM4BTX) as an excitation source, 10× (Olympus, Japan) infinity corrected objective lens and a convex lens. The fluorescence interference cube incorporates an excitation band pass filter (Semrock, USA; 430–490 nm), a beam splitter (Semrock, USA; 506 nm), and a fluorescence band pass filter (Semrock, USA; 513–555 nm).

Overall, the system operates as follows (Fig. 1): When fluorescent particles are placed inside the cavity of the acoustic device, a pair of opposite transducers is stimulated to create a standing wave causing particles to agglomerate at the nodes and form a pattern. In order to detect this pattern optically, a narrow light beam generated by the LED is passed through the excitation filter and reflected by the beam splitter to the objective lens, which focuses the LED's beam onto the fluorescence particles. Fluorescent light emitted by the particles at the surface of the acoustic device is then collected by the objective lens. This light is then passed through the fluorescence filter to a convex lens which in turn focuses the image onto the active area of the application-specific integrated circuit (ASIC) imager.

The acoustic device (Fig. 2) is formed using eight piezoelectric transducers shaped into an octagonal cavity. Eight 5 mm × 5 mm plates of NCE51 Noliac ceramic lead zirconate titanate (PZT) had an alumina loaded epoxy acoustic matching layer applied. The thickness of the matching layer was optimised using a one-dimensional transmission line model to minimise the reflection of the incident waves.[9] The

[a]The first two authors contributed equally to this work.

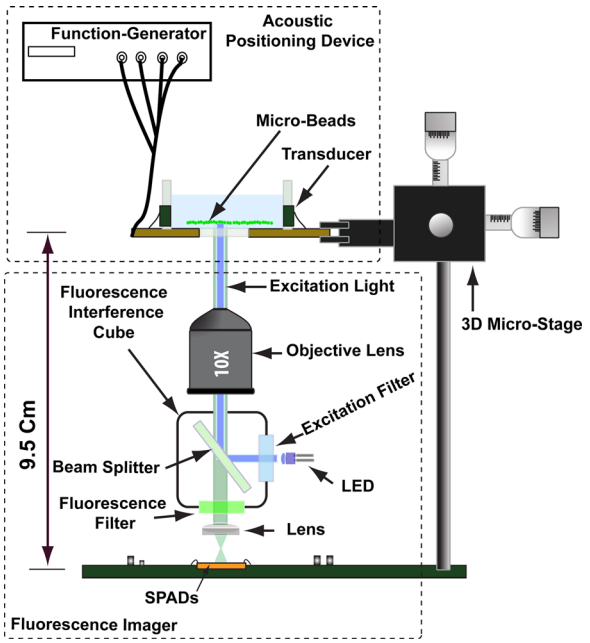

FIG. 1. Schematic of the integrated ultrasonic particle positioning and the low excitation light fluorescence imaging. The fluorescent particles are patterned by stimulating the transducers of the acoustic device. The formed patterns are directly monitored and recorded by the fluorescence imaging system.

matching layers reduce resonances that would result in unwanted standing waves with nodal positions that were fixed by the geometry, thus inhibiting translation of the field by phase variation. Matched plates without a backing layer were sufficient for the aims of this work. The matched plates were bonded to a flexible kapton ribbon that was then folded into an octagon.[10]

Synchronised transducer drive was achieved using two linked arbitrary waveform generators providing four output channels each (TGA12104, Thurlby Thandar Instruments, UK), allowing independent control of the amplitude, phase, and frequency of each channel, controlled GPIB interface using software custom written in Labview. The signals from the waveform generators were amplified and matched by high speed buffers (AD811 Analog Devices USA; BUF634T, Texas Instruments, USA). Patterning of microparticles was demonstrated both experimentally and by using a computational model to predict the pressure fields. The wave field generated by one transducer, $g(r)$, was modelled as the sum of several cylindrical point sources, $f(r)$ using Huygen's principle

$$f(r) = Ae^{\frac{-\alpha r}{\lambda}}\cos(\omega t - kr + \Phi), \tag{1}$$

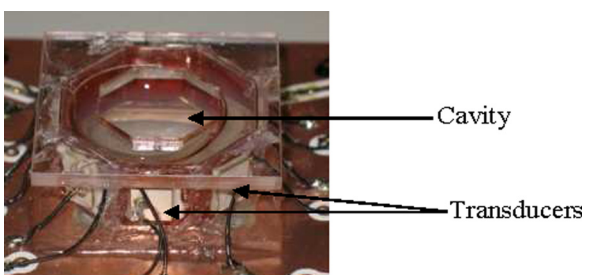

FIG. 2. Photograph of the octagonal acoustic manipulator.

$$g(r) = \sum_{i=1}^{n} f(r_i), \tag{2}$$

where A is the amplitude, α is the damping factor, λ is the wavelength, and Φ is the initial phase. The device boundaries were assumed to be perfectly absorbing.

The key component in the fluorescence detector part of the system is an ASIC imager based on a 32×32 SPAD array (Fig. 3(a)). The ASIC was fabricated according to our own design using a high voltage 0.35 μ-CMOS process from Austriamicrosystems (Germany). The SPAD is an avalanche photodiode reverse-biased above its breakdown voltage to operate in Geiger Mode and thus generates pulses proportional to the number of photons incident upon the active area of each SPAD.[7]

The physical structure of the SPAD fabricated in this chip is based on diffused guard ring junction as illustrated in Fig. 3(b). Since the CMOS process is a planar fabrication process, the p-n junction has small curvature around its edges which results in higher electric field in the edges of the p-n junction than the main active area. As a result, in high fields near to avalanche breakdown, the edges will breakdown at lower voltages than the main area. To avoid this premature breakdown, a guard ring of a lower doped material, the same as the anode, is diffused around the edges of the active area. The lower doped material reduces the electric field at the

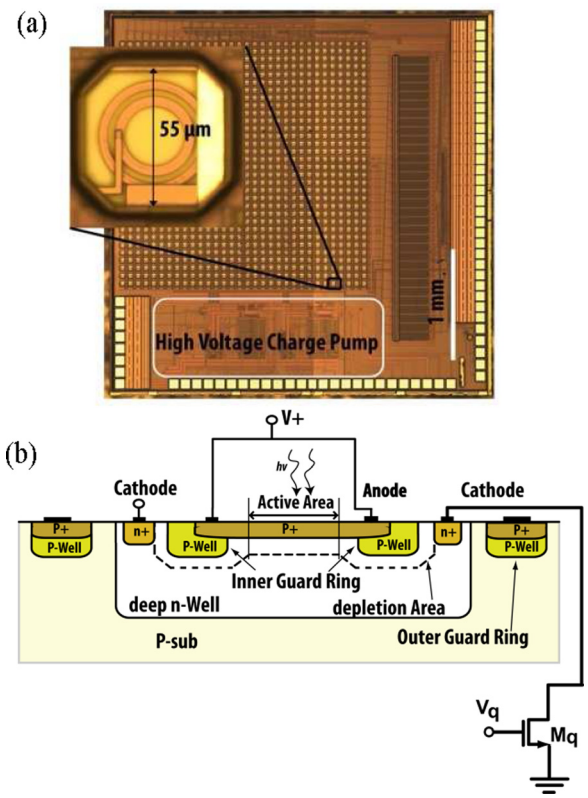

FIG. 3. (a) Photograph of the 3.7 mm × 3.7 mm ASIC chip. The imager active area is 2.4 mm × 2.4 mm. The ASIC incorporates: 32 × 32 SPAD pixels, controllable charge pump (3-37.9 V), column multiplexer, 32× (16-bit) digital pulse counters, and readout multiplexer. (b) Cross section through the centre of a circular SPAD showing the guard ring of low doped material used to reduce the electric field at the edges and corners. For each SPAD, the active area is 24 μm diameter, and the overall area including the guard ring is 55 μm in diameter.

edges hence preventing premature breakdown. Similarly, as the typical layout of a p-n junction is rectangular, higher fields occur in the corners. In order to avoid these high electrical fields in the corners, the SPAD has a circular layout creating a smooth edge, hence generating a uniform electric field across the active area.

The ASIC uses a "rolling shutter" readout arrangement, in which one 32-pixel column at a time is powered via a column multiplexer, and the pulse output from the column's SPADs during a defined counter gate period is counted by an array of 32 16-bit counters. A row mutiplexer then permits serial readout of pulse counts from the counters. The ASIC operation has been evaluated experimentally. The SPAD's Photon Detection Efficiency (PDE) spans between blue–green region and has a peak of 42.4% at 475 nm when biased at 3.1 V above its 18.9 V breakdown voltage. At dark conditions, the average dark count of the SPAD is ca. 7 kcps. Fig. 4(a) shows a grey scale representation of the dark count rates of the SPAD array. At high illumination, a single SPAD of the 1024 SPADs in the array can generate up to 4000 kcps before it reaches saturation. The ASIC is powered by a 3 V power supply and draws a maximum current of 1.74 mA.

Prior to using the imaging system to detect patterned fluorescent particles, we determined the minimum fluorescent particle concentration that can be detected by the SPAD imager. This operating parameter was set by choosing a bias point for the LED that gave an average count rate twice the dark count. In practice, this was achieved by trying different concentrations of 10 μm diameter fluorescent polystyrene particles (Polysciences Europe, Germany). At LED bias point 2.6 V (3.6 mA), measurements in Fig. 4(b) shows that the imager can efficiently detect a minimum of 1.3×10^6 particles/ml and produces more than 21.5 kcps, which is more than twice the average dark count.

Patterning experiments were performed by stimulating the acoustic transducers at 4.00 MHz sine-wave with amplitude 8 V_{pp}. At this frequency, the wavelength of the sound waves in water was $\lambda = 375\ \mu$m. By using a relatively low fluorescent concentration of 2.6×10^6 particles/ml and biasing the LED excitation source at 2.6 V (3.6 mA), we were able to detect the formed patterns on the cavity of the acoustic device reliably. Fig. 5 (left hand side) shows the computer simulation results of the acoustic landscape obtained with two transducers at different orientation and the corresponding experimental results

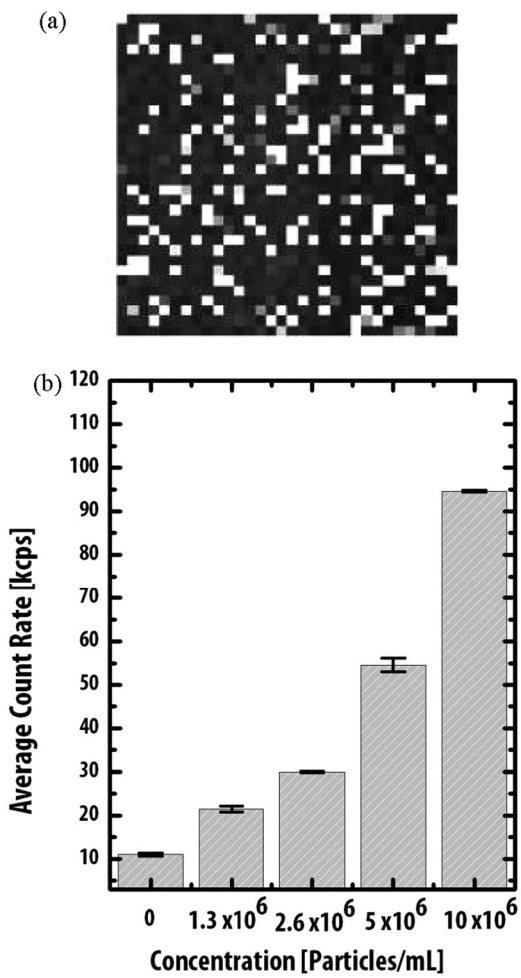

FIG. 4. (a) Grey scale image from the SPAD array in the dark, showing the fixed pattern noise. (b) A graph of the average count rate from the SPADs in the array as a function of particle concentration in the suspension place into the acoustic system with no stimulation. The inner graph shows the time response of a single SPAD to fluorescence emission.

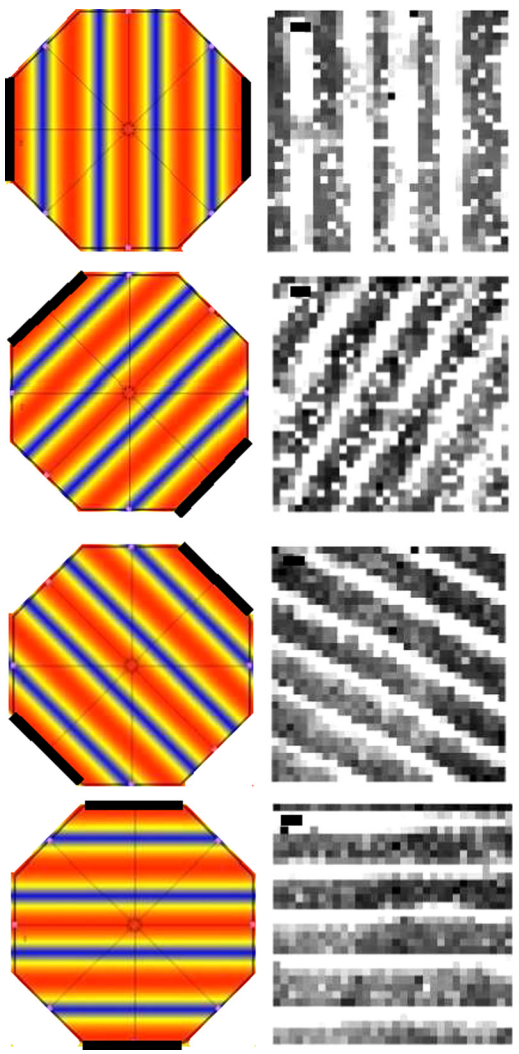

FIG. 5. Computer simulations and experimental observations of the acoustic landscape obtained with two transducers when they are excited in phase. For each figure, the simulation is on the left and the experimental results using 10 μm fluorescent polystyrene particles are on the right. The active transducers are shown in black bold line on the simulation. In the simulation, the acoustic potential energy maxima are in red, and the acoustic energy minima are in blue. (Scale bar = 100 μm for the right-hand side images.)

(right hand side). For two active transducers, a linear pattern of nodes and antinodes is formed. The distance d between the nodes is $d = 188\ \mu$m, as expected. It can be seen from the computational results in Fig. 5 that regular standing wave patterns are achieved in the middle of the octagonal cavity at the intersection of the travelling waves. The micro-particles are trapped at the minima of the potential acoustic energy density.[11] It can be seen that the patterning of the trapped particles experimentally follows this behaviour.

In conclusion, we have presented a compact, low power-excitation, fluorescence imager used in conjunction with acoustic pattering. The integrated system has been shown to pattern micro-fluorescence particles and simultaneously monitor and record the formed pattern using SPAD array imager. The high sensitivity of the SPAD array allows performing fluorescence imaging using an LED as an excitation source that was biased at low level. This opens the door for applications that requires fluorescence imaging of pattering process at low excitation levels such as cell engineering and cell culturing. Future work will involve SPADs array imager integrated directly into acoustic manipulator for cell patterning and cell physiology monitoring.

[1]A. Bernassau, F. Gesellchen, P. MacPherson, M. Riehle, and D. Cumming, Biomed. Microdevices **14**, 559–564 (2012).
[2]B. Vanherberghen, O. Manneberg, A. Christakou, T. Frisk, M. Ohlin, H. M. Hertz, B. Onfelt, and M. Wiklund, Lab Chip **10**, 2727–2732 (2010).
[3]M. Castellarnau, N. Zine, J. Bausells, C. Madrid, A. Juarez, J. Samitier, and A. Errachid, Sens. Actuators B **120**, 615–620 (2007).
[4]M. Castellarnau, N. Zine, J. Bausells, C. Madrid, A. Jua¡rez, J. Samitier, and A. Errachid, Mater. Sci. Eng., C **26**, 405–410 (2006).
[5]M. Nakao, S. Inoue, R. Oishi, T. Yoshinobu, and H. Iwasaki, J. Ferment. Bioeng. **79**, 163–166 (1995).
[6]T. Nishigaki, C. D. Wood, K. Shiba, S. A. Baba, and A. Darszon, Biotechniques **41**(2), 191–197 (2006).
[7]G. F. D. Betta, L. Pancheri, and D. Stoppa, in *High-Sensitivity Photodetectors in CMOS Technology for 3-D Imaging* (IEEE Lasers and Electro-Optics Society, 2008), pp. 354–355.
[8]M. A. Al-Rawhani, D. Chitnis, J. Beeley, S. Collins, and D. R. Cumming, IEEE Trans. Biomed. Eng. **60**, 55–62 (2013).
[9]C. R. P. Courtney, C. K. Ong, B. W. Drinkwater, A. L. Bernassau, P. D. Wilcox, and D. R. S. Cumming, Proc. R. Soc. London **468**, 337–360 (2012).
[10]A. L. Bernassau, C. R. P. Courtney, J. Beeley, B. W. Drinkwater, and D. R. S. Cumming, Appl. Phys. Lett. **102**, 164101 (2013).
[11]A. Bernassau, P. MacPherson, J. Beeley, B. W. Drinkwater, and D. Cumming, Biomed. Microdevices **15**, 289–297 (2013).